铝/钢光纤激光填充粉末熔钎焊接头界面组织与力学性能

赵旭东， 肖荣诗
(北京工业大学 激光工程研究院，北京 100124)


赵旭东

摘 要：采用经积分镜整形为矩形的光纤激光光斑，对AA6061/镀锌钢异种金属接头进行了激光填充粉末熔钎焊连接，并分析了接头连接界面的显微组织及其对接头力学性能的影响. 结果表明，选择优化的焊接参数，获得了成形饱满、无裂纹气孔等缺陷的焊缝；熔钎焊接头的金属间化合物组织由层状和枝晶状两部分组成. 层状金属间化合物组织由 Fe_2Al_5 组成，枝晶状金属间化合物组织由 τ1($Al_2Fe_3Si_3$) 和 Fe_4Al_{13} 组成；拉伸试样均断裂在钎料/镀锌钢界面，断口呈脆性断裂特征. 接头机械抗力水平由连接界面宽度与金属间化合物层最大厚度的比值决定.

关键词：异种金属；熔钎焊接；填充粉末；显微组织；力学性能
中图分类号：TG456.7 **文献标识码**：A **文章编号**：0253-360X(2013)05-0041-04

0 序 言

铝合金是目前汽车轻量化制造的主要工程材料[1]. 选用铝合金替代部分钢是一种经济合理的解决办法. 对于汽车制造来说，焊接仍是结构件连接的主要手段，但在焊接过程中生成的脆性 Fe-Al 金属间化合物严重影响了接头性能[2].

由于激光具有能量密度高和热输入量可控的特点，可以缩短铝/钢界面的反应时间来较好的抑制 Fe-Al 金属间化合物的生成，因此激光熔钎焊方法受到了广泛的研究. 试验的接头形成主要有以下两种：(1) 激光作用在钢板上[3,4]；(2) 激光作用在铝合金板上[5-8]. 以上两种方法中，激光束作用在钢母材时的激光能量利用率较高，但这种方法限制了铝/钢界面的宽度. 铝合金母材直接被激光束加热熔化时，虽然通过多种焊接布置方案可以获得尺寸较大的接头，但由于铝合金对激光的吸收率较低，焊接中激光能量的利用率较低. 为在有效控制金属间化合物层生长的同时，增加激光能量的耦合效率，采用经积分镜整形为矩形的光纤激光对 AA6061/镀锌钢板进行填充粉末熔钎焊连接试验，并分析了熔钎焊接头连接界面的显微组织及其对接头力学性能的影响.

收稿日期：2012-04-20
基金项目：国家自然科学基金资助项目(50875005)；北京市自然科学基金资助项目(3102005)

1 试验方法

试验中采用规格为 100 mm×50 mm×1.5 mm 的镀锌钢板，镀锌层厚度约 10 μm，AA6061-T6 铝合金板的规格为 100 mm×50 mm×1.2 mm. 填充粉末为 AlSi12. 选用厚度为 0.15 mm 的 BAl88Si 作为钎料. 所用材料的化学组成如表 1 所示. 焊前采用丙酮去除镀锌钢板、铝合金板和钎料表面的油脂后进行干燥.

焊接设备为 YLS-6000 型掺镱光纤激光器，最大输出功率 6 000 W. 圆形激光束经焦距为 200 mm 的铜质积分镜整形为矩形匀强光斑，焦点位置的光斑尺寸为 0.6 mm×5.8 mm. 设计了与矩形激光光斑相匹配的宽带送粉喷嘴，粉末束出口宽度为 6 mm. 焊接试样采用搭接接头形式，焊接中未使用钎剂. 接头具体布置方式为铝板在上，镀锌钢板在下，两板之间铺展一层钎料. 激光束垂直入射到铝合金板表面，送粉喷嘴与激光束的夹角为 45°. 粉末送入方向与焊接方向一致，如图 1 所示.

焊后截取接头试样，经 Keller 试剂腐蚀后由光学显微镜观察. 采用电子探针显微分析仪(EPMA)、(透射电镜) TEM 和 X-射线衍射(XRD) 对焊缝中界面组织进行观察并分析. 由于金属间化合物组织的脆性和厚度，TEM 和 XRD 试样截取了沿焊缝方向的水平截面.

将焊件按图 2 所示尺寸截取拉伸试样，在 MTS-

表 1 试验用材料的化学组成(质量分数,%)

Table 1 Chemical compositions of materials used

		Si	Fe	Cu	Mn	Mg	Cr	Zn	Ti	Al	C	P	S	Fe	Ni
铝合金	AA6061	0.52	0.5	0.18	0.09	0.84	0.22	0.16	0.13	余量	—	—	—	—	—
	填充粉末	12	—	—	—	—	—	—	—	余量	—	—	—	—	—
	钎料	12	—	—	—	—	—	—	—	余量	—	—	—	—	—
镀锌钢	母材	0.03	—	—	0.40	—	—	—	—	—	0.08	0.025	0.02	余量	—
	镀层	—	—	—	—	—	—	余量	—	—	—	—	—	—	10 ~ 15

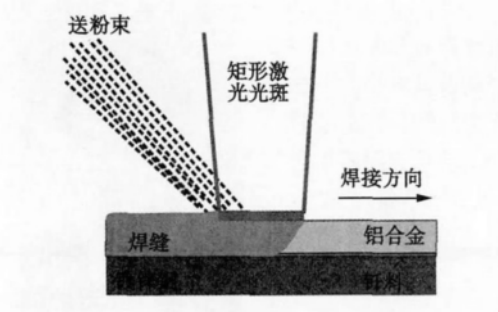

图 1 激光填粉熔钎焊试验布置图

Fig. 1 Experiment setup of laser fusion welding-brazing with filler powder

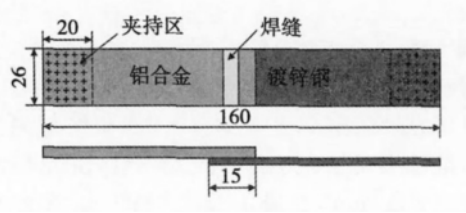

图 2 拉伸试样尺寸(mm)

Fig. 2 Dimensions of tensile specimen

810 型材料测试系统进行室温拉伸试验,拉伸速度为 1 mm/min. 在扫描电子显微镜(SEM)上观察其断口,并在 XRD 上分析断口界面组成.

2 结果与分析

2.1 金属间化合物组织

图 3 所示为 AA6061/镀锌钢激光填粉熔钎焊接头的横截面成形和连接界面金属间化合物组织形貌. 从图 3a 中可以看出,焊缝成形饱满、无裂纹气孔等缺陷. 铝合金材料熔化后铺展在镀锌钢表面,

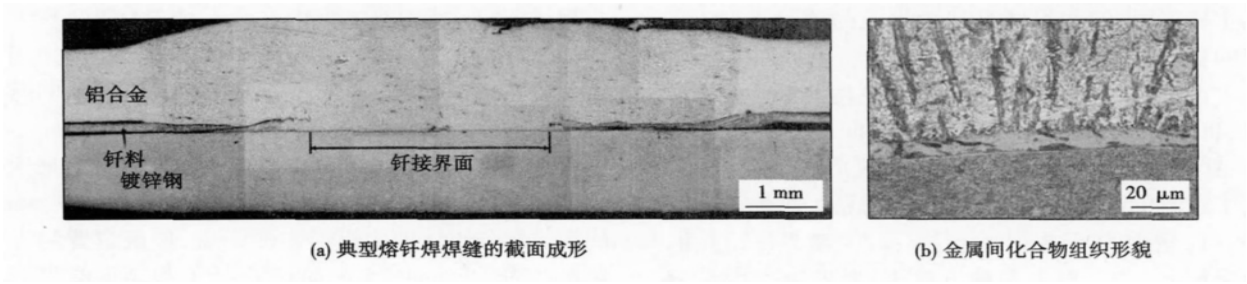

(a) 典型熔钎焊焊缝的截面成形 (b) 金属间化合物组织形貌

图 3 典型熔钎焊焊缝的截面成形

Fig. 3 Cross section of joint and OM image of intermetallic compounds layer

钢板未熔化,为典型的熔钎焊接头.

图 3b 所示为 AA6061/镀锌钢熔钎焊接头的金属间化合物组织形貌. 从图 3b 中可以看出,接头连接界面上生长有金属间化合物组织,根据其形态可分为两部分:界面上的层状组织和向上生长的枝晶状组织. 图 4 所示为金属间化合物组织的 EPMA 分析结果. 从图 4 中可以看出层状和枝状晶组织中的主要元素是 Fe 和 Al,Si 元素的含量较少. 在枝状晶组织周围的铝合金组织和枝状晶化合物中,都存在 Si 元素的富集. Fe 元素只分布在金属间化合物中.

沿焊缝的水平截面,对金属间化合物组织中枝晶状组织进行了 TEM 分析. 图 5 所示为构成枝状晶化合物的 TEM 形貌(图 5a)和衍射图样(图 5b). 由于试样的截取方向几乎与枝状晶生长方向垂直,因此在 TEM 中观察到的形貌是枝晶状组织的横截面. 试验结果发现,在枝状晶组织中发现了 τ1($Al_2Fe_3Si_3$)和 Fe_4Al_{13}. 这表明枝晶状组织是由 Fe-Al 和 Al-Fe-Si 系统化合物组成混合组织.

采用同样的方法,截取金属间化合物中层状组织进行了 XRD 分析. 分别分析了层状化合物的相

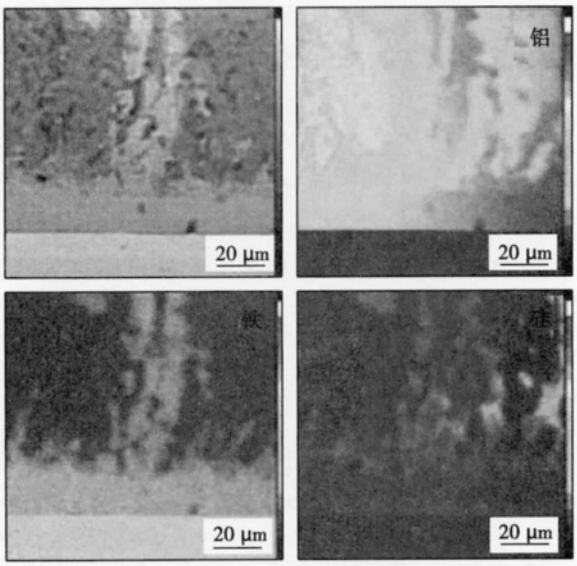

图 4　金属间化合物层中 Al，Fe，Si 元素分布

Fig. 4　Distribution of aluminum, iron and sillicon in intermetallic compounds layer analyzed by EPMA

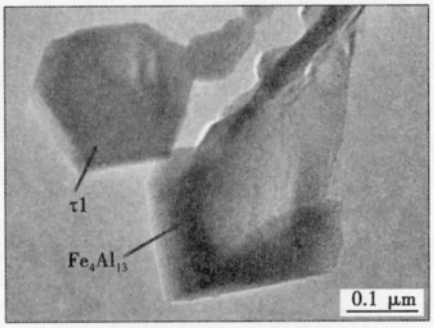

(a) τ1和Fe_4Al_{13}的TEM形貌

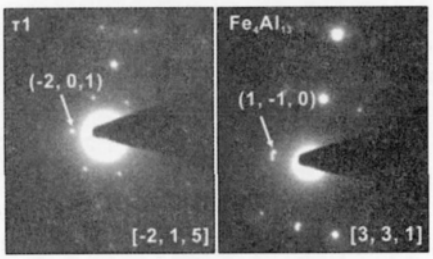

(b) τ1和Fe_4Al_{13}的衍射图样

图 5　τ1 和 Fe_4Al_{13} 的 TEM 形貌和衍射图样

Fig. 5　TEM micrograph and diffraction patterns of τ1 and Fe_4Al_{13}

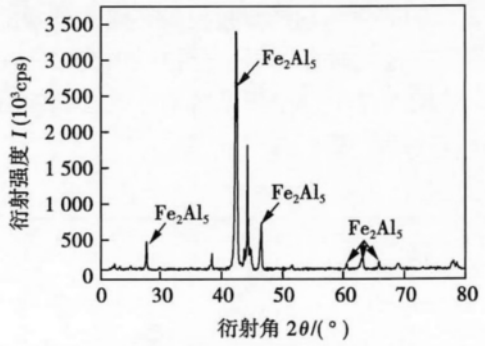

图 6　层状金属间化合物中的 Fe_2Al_5

Fig. 6　Fe_2Al_5 in intermetallic compounds layer

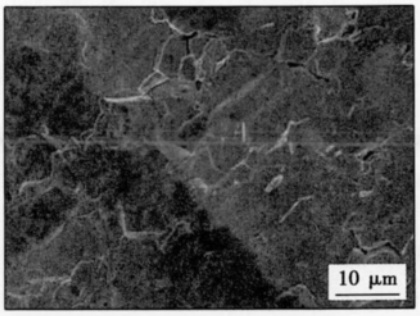

(a) 拉伸断口的SEM形貌

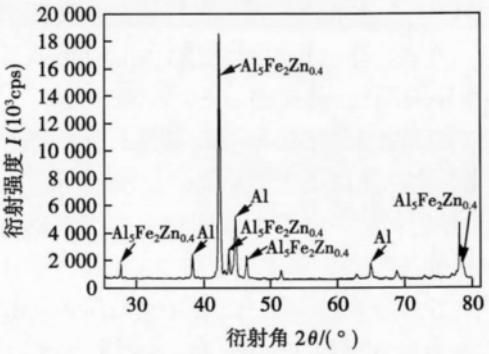

(b) 拉伸断口表面的相组成

图 7　拉伸断口铝一侧 SEM 形貌和 XRD 分析结果

Fig. 7　SEM image of fracture surface and XRD analysis results

组成. 图 6 所示为 XRD 分析结果. 从图 6 中可以看出 Fe_2Al_5 是构成层状化合物的主要组成相.

2.2　拉伸试验

拉伸试验中，试样均断裂在钎料/镀锌钢界面，采用 SEM 观察了断口表面，发现断口平整而光亮，具有明显的解理台阶和解理面，这表明接头脆性较大，呈脆性断裂特征，如图 7a 所示. 采用 XRD 分析了铝合金一侧的拉伸断口，结果表明断口表面的相组成为 $Al_5Fe_2Zn_{0.4}$ 和 α-Al，如图 7b 所示.

在激光功率为 6 000 W，焊接速度为 0.48 m/min，离焦量为+30 mm 的条件下，接头的机械抗力可达 152 N/mm. 通过调整焊接工艺参数，能够获得具有不同钎焊界面宽度(W) 和不同形态金属间化合物的焊缝. 定义焊缝中心层状和枝晶状金属间化合物组织厚度最大处的总厚度为 T_{total}. 图 8 所示为 W/T_{total} 与接头机械抗力的关系，可以看出随着比值的增大，机械抗力逐渐增加. 分析认为较宽的 W 有助于接头机械抗力的提高，而较厚的金属间化合物组织则恶化接头的力学性能. 连接界面的宽度与金

属间化合物的生长均随焊接时的热输入的增加而增大. 热输入过大时金属间化合物组织使焊缝在焊后开裂. 热输入过小时连接界面未形成有效的冶金结合而无法形成焊缝.

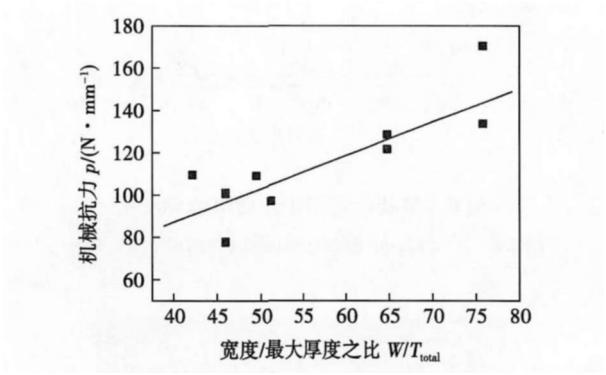

图 8 W/T_{total} 与接头机械抗力的关系

Fig. 8 Relation between W/T_{total} and mechanical resistance

根据金属间化合物组织的形态和相组成,分析认为层状金属间化合物组织是决定接头力学性能的关键. 根据物相分析,连接界面上金属间化合物组成为 $Al_5Fe_2Zn_{0.4}$ 和 Fe_2Al_5. 在快速加热冷却的焊接过程中,$Al_5Fe_2Zn_{0.4}$ 在短时间内(<1 s)形核长大成尺寸各异的晶粒,分布在 α-Fe 晶粒的上部[9],并与层状金属间化合物中的 Fe_2Al_5 相接. 相比纯金属,金属间化合物的晶体结构更加复杂,这导致了其高硬度和低塑性的特征. 由于金属间化合物组织的硬度较大,在拉伸过程中易形成应力集中. 而 α-Fe 与 Fe_2Al_5 在强度、韧性方面的差异,使得接头易从 Fe_2Al_5 组织起裂,并通过 $Al_5Fe_2Zn_{0.4}$ 相扩展,如图 9 所示.

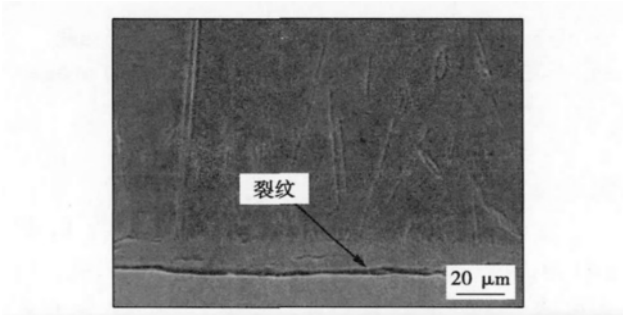

图 9 金属间化合物层处的裂纹

Fig. 9 Cracks on weld interface

3 结 论

(1) 采用经积分镜整形为矩形的光纤激光实现了 AA6061/镀锌钢异种金属接头的填粉熔钎焊连接. 选择优化的焊接工艺,获得了接头成形饱满、无裂纹气孔等缺陷的焊缝. 接头机械抗力达到 152 N/mm.

(2) 熔钎焊接头的金属间化合物组织由层状和枝晶状两部分组成. 层状化合物组织的主要组成相为 Fe_2Al_5,枝晶状组织由 τ1 和 Fe_4Al_{13} 组成.

(3) 拉伸试样均断裂在钎料/镀锌钢界面,断口呈脆性断裂特征. 接头机械抗力水平由连接界面宽度与金属间化合物层最大厚度的比值决定.

参考文献:

[1] Schubert E, Klassen M, Zerner I, *et al*. Light-weight structures produced by laser beam joining for future applications in automobile and aerospace industry [J]. Journal of Materials Processing Technology, 2001(115): 2-8.

[2] Agudo L, Eyidi D, Schmaranzer C H, *et al*. Intermetallic FexAly-phases in a steel/Al-alloy fusion weld [J]. Journal of Mechanical Science, 2007, 42: 4205-4214.

[3] Borrisutthekul R, Yachi T, Miyashita Y, *et al*. Suppression of intermetallic reaction layer formation by controlling heat flow in dissimilar joining of steel and aluminum alloy [J]. Materials Science and Engineering A, 2007(467): 108-113.

[4] Tadashi T, Sachio K, Yousuke K, *et al*. Fluxless joining of aluminium alloy to steel by laser irradiation method [J]. Welding International, 2009, 23(5): 316-322.

[5] Peyre P, Sierra G, Deschaux-Beaume F, *et al*. Generation of aluminium-steel joints with laser-induced reactive wetting [J]. Materials Science and Engineering A, 2007(444): 327-338.

[6] 彭 利, 周惦武, 吴 平, 等. 镀锌钢-6016 铝合金异种金属加入中间夹层铅的激光焊接 [J]. 焊接学报, 2011, 32(12): 81-84.
Peng Li, Zhou Dianwu, Wu Ping, *et al*. Laser lap welding of zinc-coated steel and 6016 aluminum alloy with Pb interlayer [J]. Transactions of the China Welding Institution, 2011, 32(12): 81-84.

[7] 姚 伟, 巩水利, Steve Shi. 铝合金激光双光点焊接工艺特性 [J]. 焊接学报, 2007, 28(4): 108-112.
Yao Wei, Gong Shuili, Steve Shi. Twin spot laser welding characteristics of aluminum alloy [J]. Transactions of the China Welding Institution, 2007, 28(4): 108-112.

[8] 雷 振, 于 宁, 游爱清, 等. 5A02 Q235 钢 NdYAG 激光脉冲 MIG 复合热源熔钎连接 [J]. 焊接学报, 2008, 29(6): 21-24.
Lei Zhen, Yu Ning, You Aiqing, *et al*. Fusion brazing joining for dissimilar metals between 5A02 aluminium alloy and Zn coated steel based on laser MIG hybrid welding [J]. Transactions of the China Welding Institution, 2008, 29(6): 21- 24.

[9] Giorgi M, Guillot J. Theoretical model of the interfacial reactions between solid iron and liquid zinc-aluminium alloy [J]. Journal of Materials Science, 2005(40): 2263-2268.

作者简介: 赵旭东,男,1983 年出生,博士研究生. 主要从事激光现代制造技术方面的研究. 发表论文 5 篇. Email: woody0412zxd@yahoo.com.cn

通讯作者: 肖荣诗,男,教授,博士研究生导师. Email: rsxiao@bjut.edu.cn

ized by weighted probability addition of the probability densities. Seam recognition cases are studied to demonstrate the feasibility of the fusion algorithm. The result demonstrates that the algorithm performs well in terms of recognizing the weld seam edges with precision and stability.

Key words: weld seam recognition; multi-feature; visual sensing; image processing; information fusion

Layered composite of solidified TiC-TiB_2 ceramic to Ti-6Al-4V alloy achieved by fusion bonding SONG Yalin, ZHANG Long, ZHAO Zhongmin, MA Tao (Teaching and Research Section of Mechanical Manufacturing, Department of Vehicle and Electric Engineering, Ordnance Engineering College, Shijiazhuang 050003, China). pp 37-40

Abstract: By introduction of Ti-6Al-4V plate at the bottom of combustion system in high-gravity field, fusion bonding of TiC-TiB_2 ceramic to Ti-6Al-4V alloy was achieved. The solidified TiC-TiB_2 ceramic with fine grains was prepared by combustion synthesis. Furthermore, the ceramic to titanium layered composite with chemical composition gradient was obtained. The microstructure of fusion bonding of TiC-TiB_2 ceramic to Ti-6Al-4V alloy indicates that, the presence of chemical reaction in explosive combustion and the subsequent thermal vacuum induced by liquid products in high-gravity field make Ti alloy partially fused. Then atomic inter-diffusion occurs spontaneously between liquid ceramic and molten Ti alloy, resulting in the achievement of the joint. Microstructure analysis shows that in the bonding joint, titanium riched carbides are distributed homogeneously with fine TiB_2 grains embedded in the matrix of Ti alloy. Shear strength of 450 MPa±35 MPa is achieved between the ceramic and Ti alloy. Vickers hardness decreases linearly from the ceramic to Ti alloy.

Key words: layered composite of ceramic to metal; combustion synthesis; high gravity field; fusion bonding; atomic interdiffusion

Microstructure and mechanical properties of aluminum alloy and galvanized steel joints by fiber laser fusion welding-brazing using a rectangular spot with filler powder ZHAO Xudong, XIAO Rongshi (Beijing University of Technology, Institute of Laser Engineering, Beijing 100124, China). pp 41-44

Abstract: Fluxless fiber laser fusion welding-brazing with rectangular spot was used to produce joints between 6061-T6 aluminum alloy and galvanized steel with filler powder. The joints were evaluated by metallurgical analysis and mechanical properties testing. The results indicated that favorable joint with good figuration, no crack and pore were present with optimized welding parameters. Furthermore, the joint was characterized by layered and dendritic microstructure. The layered structure is composed of Fe_2Al_5. The dendritic part is identified as $\tau 1$ and Fe_4Al_{13} phases. In addition, failures were observed in the weld/steel interface with brittle characteristics from the tensile test. The mechanical resistance of the joint is determined by the ratio of width of weld interface and the maximum thickness of intermetallic compounds layer.

Key words: dissimilar alloys; fusion welding-brazing; filler powder; microstructure; mechanical properties

Welding residual stress analysis of high-speed train undercarriage deformation by ultrasonic method MA Ziqi[1], LIU Xuesong[1], ZHANG Shiping[2], HUANG Haixia[3], FANG Hongyuan[1] (1. State Key Laboratory of Advanced Welding and Joining, Harbin Institute of Technology, Harbin 150001, China; 2. School of Electrical Engineering and Automation, Harbin Institute of Technology, Harbin 150046, China; 3. China Classification Society Industrial Corp Guangzhou Branch, Guangzhou 510235, China). pp 45-48

Abstract: Ultrasonic propagation differential method based on critical wave Lcr acoustic-elastic effect in the condition of uniaxial stress state was proposed. It raised the spatial resolution of Lcr wave stress measurement to a higher level. It was applicable in the evaluation of welding residual stress, which was a gradient stress field. Residual stress distribution in an undercarriage of high speed train with welding deformation was surveyed by this method in manufacturing shop. Residual stress in both quality and sub-quality areas were obtained and compared. The source of the contraction distortion was confirmed, and it provided reference to the working out of the shape-righting scheme.

Key words: acoustic-elastic effect; Lcr wave; propagation differential method; welding deformation; residual stress

Microstructure of matrix and wear resistance of ceramic layer of TiC/Fe surface gradient composites WANG Liangliang[1], XU Yunhua[1], ZHONG Lisheng[1,2], WANG Juan[1], YAN Honghua[1] (1. Institute of Wear-resistance Materials, School of Mechanical and Electrical Engineering, Xi'an University of Architecture & Technology, Xi'an 710055, China; 2. School of Materials Science and Engineering, Xi'an Shiyou University, Xi'an 710065, China). pp 49-53

Abstract: In this paper, the joining of gray cast iron (HT300) and titanium plate with the thickness of 0.25 mm was performed by the method of pouring. The sample was isothermally kept in vacuum tube furnace at 1 138 ℃ for 8 h, and cooled in furnace to room temperature. TiC particulates reinforced surface gradient composite was prepared on the iron matrix of cast iron surface by the in-situ technology. Microstructure analysis, microhardness and wear-resistance test were carried out on the recombination region. The experimental results show that the TiC particulates reinforced surface gradient composite is composed of three layers. The difference between the three layers lies in the different sizes and different shapes of TiC particulates. The microhardness decreases gradually from composite layer (C region) to pearlite region. The maximum microhardness appears in the high density ceramic layer (C region). Therefore, wear experiment was further performed to study wear-resistance of the high density ceramic layer of the surface gradient composite. Apparently, the wear-resistance of high density ceramic layer is enhanced greatly in comparison with gray cast iron.

Key words: TiC particulates; microhardness; ceramic layer; wear-resistance

Features extraction for weld image of scanning laser sensing LEI Zhenglong, LV Tao, CHEN Yanbin, CHEN Hong (State Key Laboratory of Advanced Welding and Joining, Harbin Institute of Technology, Harbin 150001, China). pp 54-58